ERDC/CRREL TR-22-15

US Army Corps of Engineers®
Engineer Research and Development Center

ERDC ENGINEER RESEARCH & DEVELOPMENT CENTER

ERDC 6.1 Military Engineering Program

Extracting Sintered Snow Properties from MicroCT Imagery to Initialize a Discrete Element Method Model

Taylor S. Hodgdon, Brendan A. West, Julie T. Parno, Theodore W. Letcher, Zoe R. Courville, and Lauren B. Farnsworth

September 2022

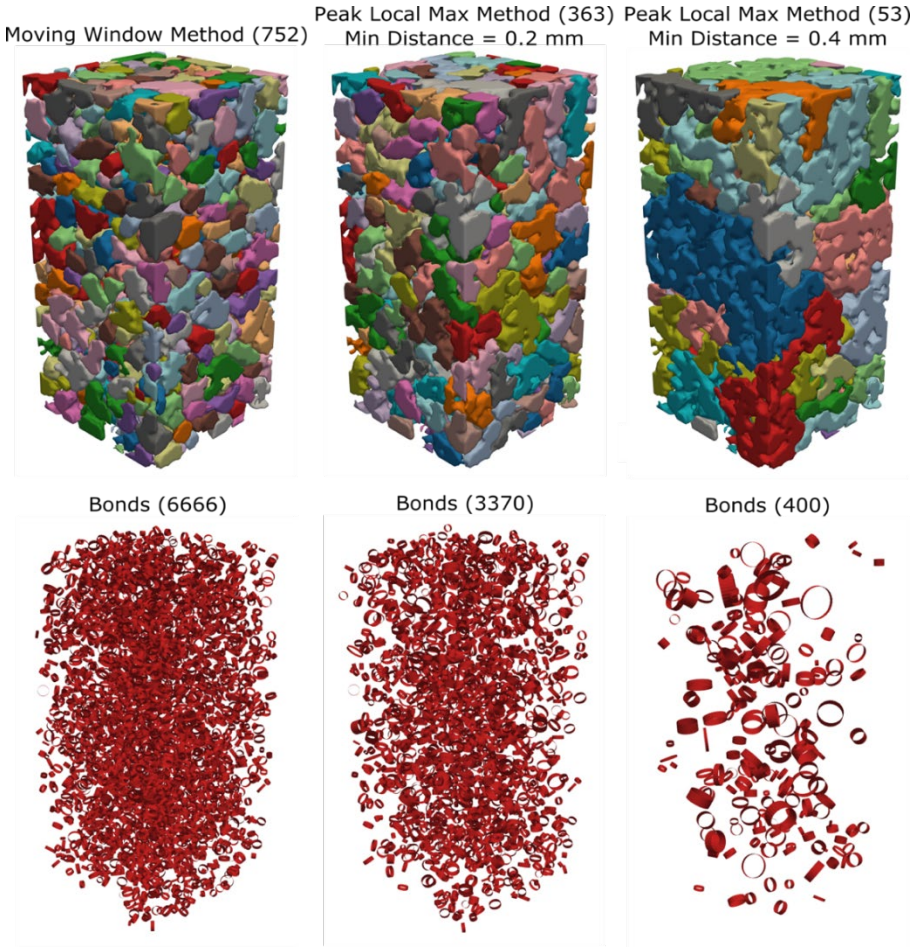

Cold Regions Research and Engineering Laboratory

The US Army Engineer Research and Development Center (ERDC) solves the nation's toughest engineering and environmental challenges. ERDC develops innovative solutions in civil and military engineering, geospatial sciences, water resources, and environmental sciences for the Army, the Department of Defense, civilian agencies, and our nation's public good. Find out more at www.erdc.usace.army.mil.

To search for other technical reports published by ERDC, visit the ERDC online library at https://erdclibrary.on.worldcat.org/discovery.

ERDC/CRREL TR-22-15
September 2022

Extracting Sintered Snow Properties from MicroCT Imagery to Initialize a Discrete Element Method Model

Taylor S. Hodgdon, Brendan A. West, Julie T. Parno, Theodore W. Letcher, Zoe R. Courville, and Lauren B. Farnsworth

US Army Engineer Research and Development Center (ERDC)
Cold Regions Research and Engineering Laboratory (CRREL)
72 Lyme Road
Hanover, NH 03755-1290

Final Technical Report (TR)

Prepared for Headquarters, US Army Corps of Engineers
Washington, DC 20314-1000

Under PE 0601102A, Project AB2, "Protection, Maneuver, Geospatial, Natural Sciences," Task SAB202, "Fundamental Adaptive Protection and Projection Research"

Abstract

Modeling snow's mechanical behavior is important for many cold regions engineering problems. Because snow's microstructure plays a significant role in its mechanical response, it is imperative to initialize models with accurate bond characteristics and realistic snow-grain geometries to precisely capture the microstructure interactions.

Previous studies have processed microcomputed tomography scans of snow samples with a watershed method to extract grain geometries. This approach relies on identification of seed points to segment each grain. Our new methodology, called the "moving window method," does not require prior knowledge of the snow-grain-size distribution to identify seed points. We use the interconnectivity of the segmented grains to identify bond characteristics. We compare the resultant grain-size and bond-size distributions to the known grain sizes of the laboratory-made snow samples. The grain-size distributions from the moving window method closely match the known grain sizes, while both results from the traditional method produce grains that are too large. We propose that the bond network identified using the traditional method underestimates the number of bonds and overestimates bond radii. Our method allows us to segment realistic snow grains and their associated bonds, without prior knowledge of the samples, from which we can initialize numerical models of the snow.

Contents

Figures and Tables

Figures

Tables

Preface

This study was conducted for Headquarters, US Army Corps of Engineers, under PE 0601102A, Project AB2, "Protection, Maneuver, Geospatial, Natural Sciences," Task SAB202, "Fundamental Adaptive Protection and Projection Research."

The work was performed by the Terrestrial and Cryospheric Sciences Branch (Dr. John Weatherly, chief), US Army Engineer Research and Development Center, Cold Regions Research and Engineering Laboratory (ERDC-CRREL). At the time of publication, Dr. Caitlin A. Callaghan was division chief. The acting deputy director of ERDC-CRREL was Dr. Bryan E. Baker, and the director was Dr. Joseph L. Corriveau.

Portions of Section 2.2 are modified and reprinted from Ross Lieblappen, John M. Fegyveresi, Zoe Courville, and Donald Albert, "Using Ultrasonic Waves to Determine the Microstructure of Snow," *Frontiers in Earth Science* 8 (February 2020):34, https://doi.org/10.3389/feart.2020.00034, public domain.

COL Christian Patterson was commander of ERDC, and Dr. David W. Pittman was the director.

This page intentionally left blank.

1 Introduction

1.1 Background

Characterization of snow microstructure is important for our understanding of the snow's mechanical strength, optical properties, and thermal conductivity. However, accurate characterization is challenging due to the temporal evolution of the physical properties of snow, such as grain size and shape, porosity, and bond size. A snowpack undergoes metamorphism due to temperature and vapor gradients, which are driven by environmental conditions and are therefore highly variable. The most common approach for characterizing the microstructure is to take a sample of the snow, image it with microcomputed tomography (microCT), and then process the resultant images. The accuracy of the processed result depends on the image analysis techniques used and can vary widely depending on user-defined parameters. In this paper, we compare a common approach for processing microCT images of snow against a novel approach.

Our motivation for capturing accurate details of snow grains and sintered bonds is to initialize numerical snow strength models with highly accurate one-to-one geometric representations of real snow microstructures. Studies have shown that the mechanical response of snow depends on the properties of its microstructure (Hagenmuller et al. 2014, 2015; Willibald et al. 2019; Willibald 2021). Therefore, the ability to replicate precise shapes, sizes, and orientations of the snow microstructure is imperative to model fidelity. However, previous snow-modeling approaches often simplify the microstructure, thereby missing important aspects of the mechanical response. For example, a popular modeling approach is the discrete element method (DEM), which is particularly useful for simulating granular materials where the interactions between individual pieces of the material, or particles, affect the material's macroscopic response. However, previous snow studies using the DEM have primarily used sphere-shaped particles for the grains and particle centroid-to-centroid cohesive bonds for the sintered bonds (Gaume et al. 2015; Mulak and Gaume 2019; Kabore and Peters 2020a, 2020b; Bobillier et al. 2020; Kabore et al. 2021; Peters et al. 2021). Although these assumptions simplify the modeling computations, they miss important aspects of the snow microstructure, such as complex and irregular grain shapes and variable sintered bonds between neighboring grains. We aim to implement a new methodology

that allows us to extract realistic snow grain and bond microstructures from images of real snow samples, from which we can initialize more accurate numerical models.

A significant advancement in characterizing the microstructure of snow came with the introduction of microCT, which allows 3D reconstruction of a snow sample (Lundy and Adams 1998). As opposed to serial sectioning, microCT is a nondestructive and relatively efficient technique and therefore has been utilized by many studies to investigate metamorphism and mechanical deformation of snow over time (Chen and Baker 2010; Coleou et al. 2001; Flin and Brzoska 2008; Hagenmuller et al. 2016; Kaempfer et al. 2005; Kaempfer and Schneebeli 2007; Krol and Löwe 2016; Schleef et al. 2014). However, the reconstruction does not differentiate individual snow grains, which is important for initializing numerical models (Hagenmuller et al. 2015; Johnson and Hopkins 2005; Kabore et al. 2021). This has led to the development of several methods for decomposing the complex ice-air images into separate grains. Documented segmentation techniques generally fall into three categories: watershed algorithms, skeletonization and morphological thinning, and curvature-driven algorithms.

The watershed segmentation method is a well-established and popular segmentation technique that originates in image analysis (Serra 1983) and was first applied to 3D meshes by Mangan and Whitaker (1999). In watershed segmentation, the approach is to treat the gray-scale values of the imagery as elevations in a topographic map. Watersheds are “flooded” until the separate drainage basins meet. For microCT images of snow, this procedure begins with a stack of binarized images (of ice and air phases) representing horizontal slices of the 3D sample. The Euclidean distance transform is then computed for the snow pixels, which is the distance from each snow pixel to the nearest air pixel. Relating back to the watershed analogy, these distance values correspond to the local slope at each pixel. Seed points are needed to determine where each basin starts flooding from and are often located at the local maxima of the distance field. Often there are more local maxima than actual grains, and therefore flooding from each of these points will result in oversegmentation. To avoid this, an additional step is often taken to subset the seed points based on their proximity to each other—if two seed points are closer than some minimum distance value, then one is removed. This approach is often referred to as the peak local maximum (PLM) method. After the seed points are defined, the wa-

tershed algorithm floods the basins around each point until the basins attributed to different seeds meet on watershed lines. In this snow microstructure application, we assume the watersheds meet at the interface between snow grains.

While the watershed segmentation method is easy to implement and can provide accurate results, there are several drawbacks. The first issue is the step where seed points are subset, as it introduces significant subjectivity to the process and depends on a user-defined threshold for the minimum distance separating these markers. Useful distance values are often based on the average grain size of the snow sample to estimate the usual distance between grain centroids. However, this is not always known a priori. The second disadvantage is that the watershed algorithm works best with spherical particles and can struggle separating the boundaries of complex snow-grain shapes (Theile and Schneebeli 2011).

The second type of image segmentation approach is based on the process of skeletonization, or reducing the grain regions in the binary image to a series of line segments that preserve the geometry and topology of the grain structures. The skeleton of the binary image is often produced using either a distance transform (Edens and Brown 1995) or through morphological thinning or erosion (Baldwin et al. 1996). Thinning occurs by eroding away pixels from the boundary of a grain until no more thinning is possible and what remains is the skeleton, also called the medial axis. Liang et al. (2000) utilized this method to characterize pore space in porous media. They found pore necks by searching through the pore-space channels and identifying local minima of the hydraulic radius. As Theile and Schneebeli (2011) point out, however, this definition of necks is not valid for dense multiparticle structures, resulting in potential inaccuracies.

Lastly, multiple segmentation processes leverage the curvature of image regions, often in combination with skeletonization or watershed methods (Brzoska et al. 1999; Hagenmuller et al. 2014; Ogawa et al. 2006; Theile and Schneebeli 2011; Wang et al. 2012; Zhang et al. 2002). Gaussian curvature is the product of the principal curvatures and can be used to identify whether a surface is convex of concave in shape within a localized region. Since sintered bonds span between two surfaces, they typically have thin concave necks. These curvature-based methods, therefore, use these locations as reasonable indicators of neck locations. However, not all surface points with a Gaussian curvature are part of a neck. Theile and

Schneebeli (2011) used a second check to determine if the cross section of each point with negative Gaussian curvature is a local minimum area by using dilation and intersecting plane minimization. By combining approaches, they improved upon the watershed and skeleton-based algorithms. Wang et al. (2012) used the sign of the principal minimal curvature (k_{min}) as a criterion, which better detects triple junctions, to separate out neck regions and granular regions that they then propagated volumetrically using Voronoi labeling. Building on this concept, Wang et al. (2014) developed a purely volumetric approach using digital flow (Dey et al. 2003).

Most recently, Hagenmuller et al. (2014) introduced a new segmentation approach that determined potential zones of mechanical weakness, identified as concavities with a significant curvature and constrictions. In their approach, they combined many of the previously described techniques. Like Wang et al. (2012), they began by distinguishing groove, neck, and crater regions from convex regions using the principal minimal curvature (k_{min}). They then applied a watershed algorithm on $-k_{min}$ and set an arbitrary threshold to avoid artificial oversegmentation. The resulting bond candidates were then dilated, and those bonds of minimal area within the dilated bond candidates were computed via a graph-cut approach (Boykov et al. 2001). The grains were simultaneously merged if they met certain criteria based on the grain surface area and contact area between both grains. While the results of this work appear qualitatively accurate, the results can be variable depending on the specified k_{min} threshold.

While advancements have been made in segmentation of 3D snow images into their constituent parts, each proposed method has some level of subjectivity and requires a balance between computational expense and accuracy. One of the greatest advantages of the watershed segmentation approach is the ease of implementation and computational efficiency. Therefore, for this work, we aim to exploit these benefits and build upon the watershed method by improving the methodology for determining seed points, tackling the greatest source of subjectivity and therefore bias in the approach. We call our approach the “moving window method” (MWM), as it passes a variable-sized “window” region throughout the image to identify and limit the number of watershed seed points.

1.2 Objectives

The primary objective of this work was to develop a methodology to extract sintered snow properties from microCT imagery to initialize a DEM framework. The first step in this process was to develop a more robust way to identify seed points for watershed segmentation. Next, we needed to build a framework for identifying the sintered-bond locations and their associated characteristics. We will use these segmented grains and bond properties to initialize the DEM framework, which will allow us to replicate laboratory tests of snow strength.

1.3 Approach

In this report, we discuss a new method, the MWM, that can be used to identify seed points for initializing a watershed segmentation. We also demonstrate how we can identify and characterize the sintered bonds in a snow sample after the segmentation process is completed. Here we test this new methodology microCT images of sintered snow with varying grain and sintered-bond-size distributions. We then compare the segmentation results of the MWM to another traditional seed-point identification technique. We validated the segmentation results for both methods using the known grain sizes of the laboratory-made snow samples. Finally, we discuss the benefits of using the new approach and highlight the importance of reliable segmentations for initializing snow-mechanics models.

2 Laboratory Methodology

2.1 Snow-sample preparation

Snow samples were created using freshly fallen snow that was stored in a cold room at 15°F. A sieve stack was used to make snow samples with three different grain sizes: small (<450 μm*), medium (450–825 μm), and mixed (50% <450 μm and 50% 450–825 μm). The mixed samples were created using the sieved snow from the small and medium samples. Following Langlois et al. (2020), we assume that each sample is represented by a log-normal size distribution. We set the peak of the small-grain-size distribution to 300 μm since smaller grain sizes are not as common in snow. The peak of the medium grain size was calculated by taking the average of the two sieve sizes used to make the sample (637.5 μm). Finally, the mixed sample grain size was calculated as the average of the small and medium distribution peak values (468.75 μm). After sieving the samples, they were packed into a 15.5 cm tall, 5 cm diameter cylinder (Figure 1) and left to rest for three days at 15°F. The samples were then removed from the Teflon cylinder and left in an open-air chamber to continue sintering at 15°F (Figure 2). Duplicate samples of each grain size were made and left to sinter for 3 to 138 days. After the sample had sintered to the desired time, the density was calculated and recorded. Table 1 shows each sample name and characteristic information.

Figure 1. Teflon cylindrical molds used to prepare the snow samples.

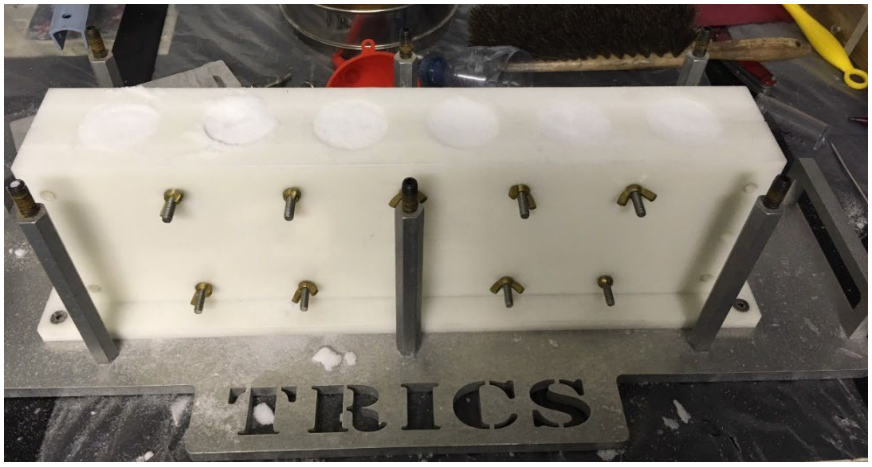

* For a full list of the spelled-out forms of the units of measure used in this document, please refer to *US Government Publishing Office Style Manual*, 31st ed. (Washington, DC: US Government Publishing Office, 2016), 248–252, https://www.govinfo.gov/content/pkg/GPO-STYLEMANUAL-2016/pdf/GPO-STYLEMANUAL-2016.pdf.

Figure 2. Snow-sample cylinder (133_mx_01) after sintering.

Table 1. Snow-sample characteristics.

Sample ID	Grain Size	Sinter Time (days)	Density (kg/m³)
003_sm_01	<450 µm	3	459.42
003_md_01	450–825 µm	3	413.8
003_mx_01	50% <450 µm and 50% 450–825 µm	3	487.49
007_sm_01	<450 µm	7	469.82
007_md_01	450–825 µm	7	455.73
007_mx_01	50% <450 µm and 50% 450–825 µm	7	506.75
017_sm_01	<450 µm	17	481.39
017_md_01	450–825 µm	17	450.28
017_mx_01	50% <450 µm and 50% 450–825 µm	17	502.55
133_sm_01	<450 µm	133	480.01
133_md_01	450–825 µm	133	418.33
133_mx_01	50% <450 µm and 50% 450–825 µm	133	423.46
138_sm_01	<450 µm	138	458.38
138_md_01	450–825 µm	138	351.55
138_mx_01	50% <450 µm and 50% 450–825 µm	138	389.02

2.2 MicroCT imaging

We used a Bruker SkyScan 1173 microCT scanner equipped with a Hamamatsu 130/300 tungsten X-ray source and a camera detector with 2240 × 2240 pixel output to scan each snow sample. The SkyScan 1173 X-ray

source produces a fixed conical, polychromatic beam with a spot size less than 5 μm. The maximum accelerating voltage of the X-ray beam was set to approximately 40 kV with a current of about 200 μA. Samples were rotated 180° in 0.3°–0.4° steps, with five-frame averaged attenuation images captured at each step using a camera exposure of about 330 ms. A 2 × 2 camera binning was used to create X-ray images of 1120 × 1120 pixels. Each sample had roughly 1000 2D slices, which could be stacked to make the full 3D reconstruction.

The images were reconstructed using Bruker SkyScan's NRecon software (version 1.7.3.1) to produce a vertical stack of gray-scale cross-section images. As part of image postprocessing, we performed ring artifact reduction, postalignment correction, beam-hardening correction, and Gaussian smoothing to reduce noise. The resulting images had a spatial resolution of roughly 20 μm per voxel and a 16-bit gray-scale dynamic range.

3 Processing MicroCT Imagery

3.1 Moving window seed-point identification

It is crucial that the seed points in the watershed segmentation algorithm closely match the true centers of each snow grain, else the process will produce inaccurate segmented results. Our methodology focuses on identifying realistic seed points that closely correspond to the centers of grains without needing a priori knowledge of the grain-size distribution. Figure 3 provides an overview of this methodology.

Figure 3. Overview of the moving window seed-point identification procedure.

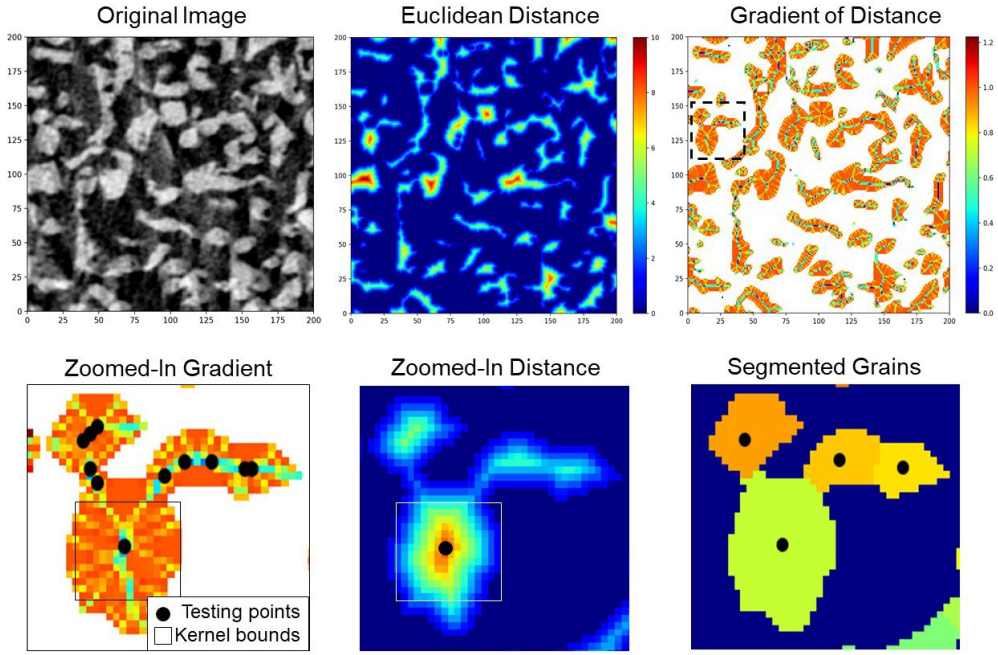

Our methodology begins with combining the 2D microCT image slices into a 3D array. This array is then binarized such that voxels containing snow are labeled with "1" and those containing nonsnow are labeled with "0." The gray-scale images are binarized into snow and nonsnow pixels by choosing the threshold value as the midpoint between the two maxima in the gray-scale histogram that indicate snow and nonsnow values. A Euclidean distance (d) is then calculated between each snow voxel and the closest nonsnow voxel, using

$$d = \sqrt{(x_1 - x_{2)}{}^2 + (y_1 - y_{2)}{}^2 + (z_1 - z_{2)}{}^2}, \quad (1)$$

where x, y, and z are the coordinates of the two voxels (subscripts 1 and 2). The result of this calculation is a 3D array containing the shortest distance between each snow voxel and the nonsnow region. The magnitude of the gradient ($||\nabla G||$) is then calculated on this Euclidean distance array using

$$||\nabla G|| = \sqrt{{G_x}^2 + {G_y}^2 + {G_z}^2}, \quad (2)$$

where $G_{x,y,z}$ are the gradients in the x, y, and z directions, respectively. Next, a set of initial test points are identified by selecting voxels from the gradient magnitude array that have a value less than t_g:

$$t_g = \mu_g - 4\sigma_g, \quad (3)$$

where μ_g is the mean gradient magnitude and σ_g is the standard deviation. This t_g calculation was selected as it is not sample dependent, and it limits the number of potential test points to only those with the lowest gradient magnitudes.

Once the test points have been identified, we create a 3 × 3 × 3 voxel "window" around each test point. If there is a nonsnow voxel within that window, the process stops. Otherwise, the window continues to grow by one voxel in each direction until the window contains at least one nonsnow voxel. Once the final window size has been determined, we collect each test point that falls within that window. We then iterate through these points and identify the point that has the combination of the largest Euclidean distance value and the lowest gradient. This voxel becomes a final seed point for the watershed segmentation, and the other test points are ignored. After the seed point has been identified, all voxels within the window are reclassified as nonsnow. This step avoids multiple seed points identified within a single grain, which would otherwise result in over segmentation.

After the final seed-point locations have been identified, we use the watershed segmentation algorithm from the Python Scikit-Image library to flood the binarized array and create a 3D grain segmentation (van der Walt et al. 2014).

3.2 Sintered-bond characterization

Accurately identifying and characterizing the sintered bonds between grains is critical for numerical models of snow, as these bonds are often

the weakest part of the snow structure and therefore play a vital role in the snow's mechanical response. Our method for identifying bonds is based on the principle that sintered bonds form primarily due to surface diffusion at the interface between touching grains. Therefore, by locating pairs of neighboring grains, the sintered-bond locations can be identified.

A set of neighboring grains is constructed by iterating over the unique grain IDs in the final segmented array from section 3.1 and finding if any of that grain's voxels are direct neighbors to voxels in another grain. In this context, we refer to the "home" grain as the grain of the current iteration and the "neighbor" grain is the grain in direct contact with the home grain. For each home and neighbor pairing, a new temporary 3D array with the same dimensions as the full image stack is created where the voxels within the home grain have a value of 1, the voxels in the neighbor grain have a value of 2, and all the other voxels in the array have a value of 1.5 (the mean value of the home and neighbor grains). The gradient magnitude is then calculated within this temporary array. The voxels with the largest gradient magnitude will be those directly on the boundary between the home and neighbor grains. Therefore, we assume that the sintered-bond region includes all voxels in the region where the gradient is largest. This process repeats for each unique pairing of a home and neighbor grain until all sintered bonds have been located (Figure 4).

Once the sintered bonds have been identified, the radii of those bonds can be calculated. We assume that the bond between two grains is approximately cylinder shaped. With this assumption, the centroid of the sintered bond is identified, then an idealized disk is created with the same volume of the bond voxel region. The radius of the idealized cylinder is used to represent the size of the sintered bond. Thus, each home and neighbor pairing has a sintered bond with an associated radius, which can be used to instantiate the bond parameters in the DEM framework.

Figure 4. Overview of the bond identification procedure.

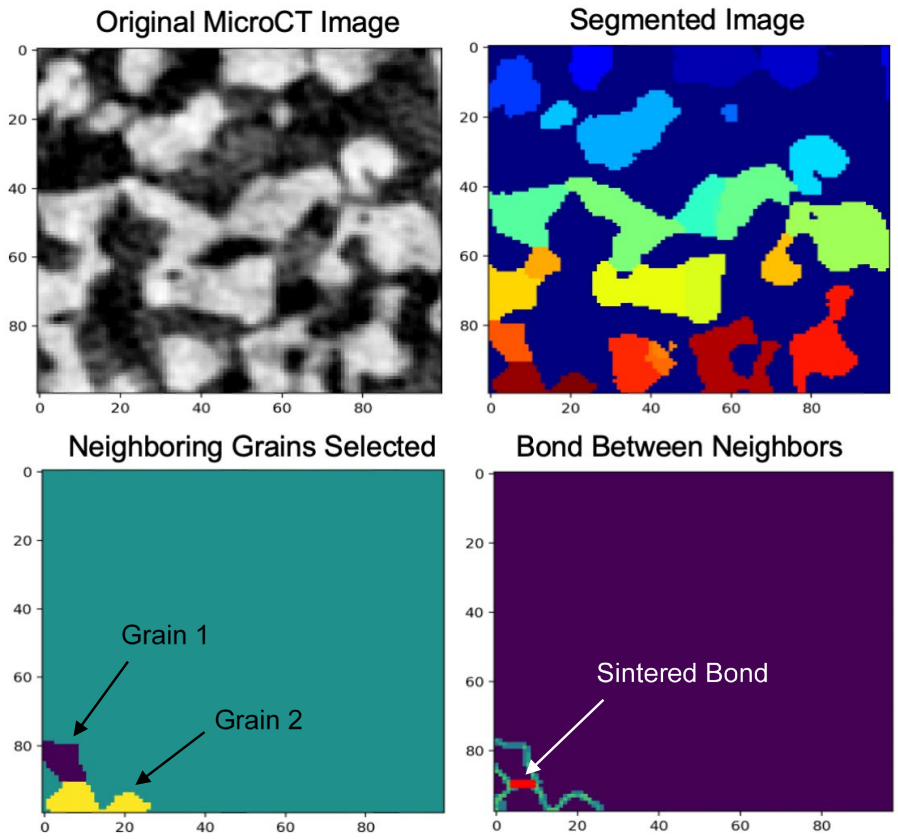

3.3 Meshing process

The next step in the modeling framework is to convert the segmented grain geometries into 3D numerical objects that can be imported into the DEM code. This process requires a couple of steps, the first of which takes the segmented images (3D arrays) and uses a Python library called PyVista (Sullivan and Kaszynski 2019) to convert the pixels of each individual grain into a disconnected point cloud. We then use PyVista functionality to create a Delaunay triangulation from the point cloud and extract the surface shell of the triangulation. This gives an approximate mesh of the grain's surface, which can be quite bumpy or contain holes due to the triangulation process and the pixel resolution. Therefore, we use another Python library called PyMeshFix (Attene 2010) to fill any holes, smooth, and fix any problems in the surface mesh. The result is a closed surface mesh approximating the surface of a specific ice grain (Figure 5).

Figure 5. Overview of the total meshing process. Image *A* shows the segmented image pixels in 3D; *B* shows the smoothed surface mesh generated with PyVista and PyMeshFix.

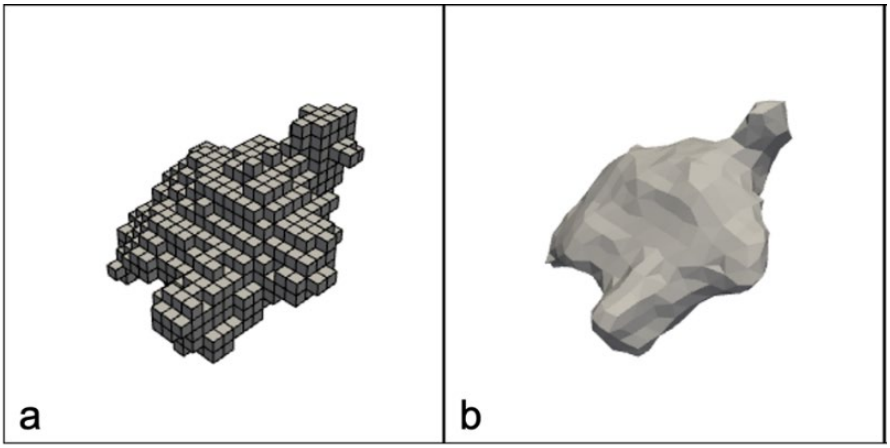

4 Results

The segmentation and bond identification methodology outlined in Section 3 produces a collection of individual snow grains and their associated sintered bonds. Figure 6 compares the 3D grain and sintered-bond results from the MWM with the results from the PLM. The sample used for this comparison was 007_sm_01, which was produced with a sieve size of 0.45 mm. In theory, this a priori knowledge of the sample informs us that the snow grains should be smaller than 0.45 mm, so we produced PLM segmentations with minimum distances that are smaller than this. The middle and right columns of Figure 6 use minimum distances of 0.2 mm and 0.4 mm, respectively.

It is clear from the comparison in Figure 6 that using different minimum distance values can produce vastly different segmentations and bond networks, thus highlighting the aforementioned issues with the PLM approach. The 0.4 mm result contains many large grains that combine several clearly discrete snow grains. In addition, the 0.2 mm result still has a number of large grains that appear to combine multiple individual snow grains. This suggests that even with a priori knowledge of the snow-sample construction, additional tuning of the minimum distance parameter is still needed to produce realistic results with PLM. In addition, the results of the PLM method will be more prone to incorrect segmentations if there is a wide range in grain sizes. Since the minimum distance specifies how far apart seed points (i.e., grain centers) must be from one another, it inherently assumes that all the grains are roughly equal size and uniform shape.

The MWM results contain significantly more grains and bonds than the PLM results; however, the results appear to qualitatively separate the grains between the concave regions where we would expect bonds to be. The higher number of bonds makes sense, as the bond identification method described above identifies one bond per pair of adjacent grains. In addition, the size distributions of the MWM grains better match the sieve sizes used to make the snow samples. Figure 7 shows the grain-size distributions produced by each segmentation approach, where the grain size is defined as the diameter of an idealized sphere of equivalent volume for each grain. As evidenced in Figure 7, the 0.4 mm PLM results have grains that are significantly larger than the 0.45 mm sieve that was used to make the sample. This could be explained by the idealized sphere assumption we chose to calculate the grain sizes. For example, if a snow grain is oblong, it

could fit through the sieve if oriented correctly. However, if we take that grain volume and instead assume it is a sphere, the diameter may be larger than the sieve size. The results of the PLM segmentation with a minimum distance of 0.2 mm had a mean grain size of 0.35 mm, with less than 30% of the grains larger than the sieve size. The MWM results, however, had a mean grain size of 0.3 mm and almost no grains identified larger than the sieve size. Thus, the grain-size distributions indicate that the MWM produced grains that closer match how the sample was prepared, with the benefit of not needing a priori knowledge of the sample.

Figure 6. Comparison of segmented and meshed results from the MWM and the PLM method using two different minimum distances. The bottom row shows the identified sintered bonds, as visualized with cylinders where the radius and lengths are calculated as described in Section 3.2. The numbers in parentheses indicate the number of segmented grains, or bonds, in the corresponding image. Note how the MWM identified a larger number of grains and corresponding bonds in the snow microstructure.

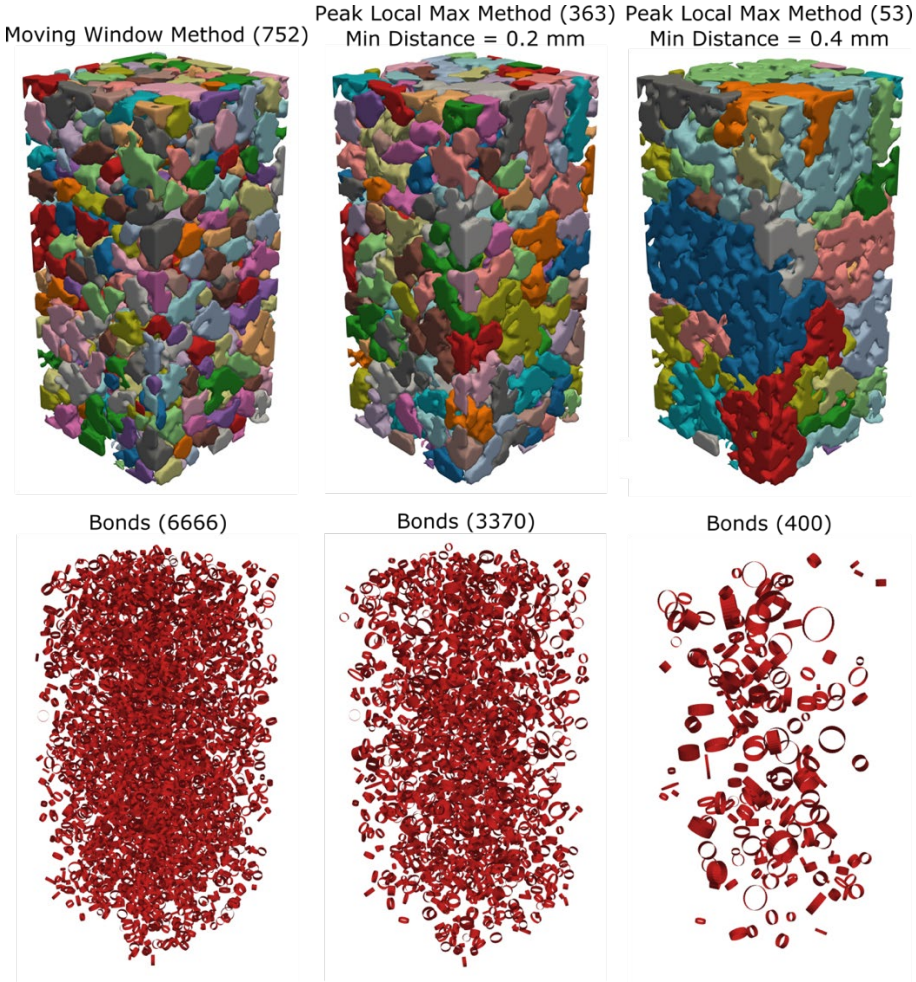

Figure 7. Grain-size distributions produced by the three different segmentation methods.

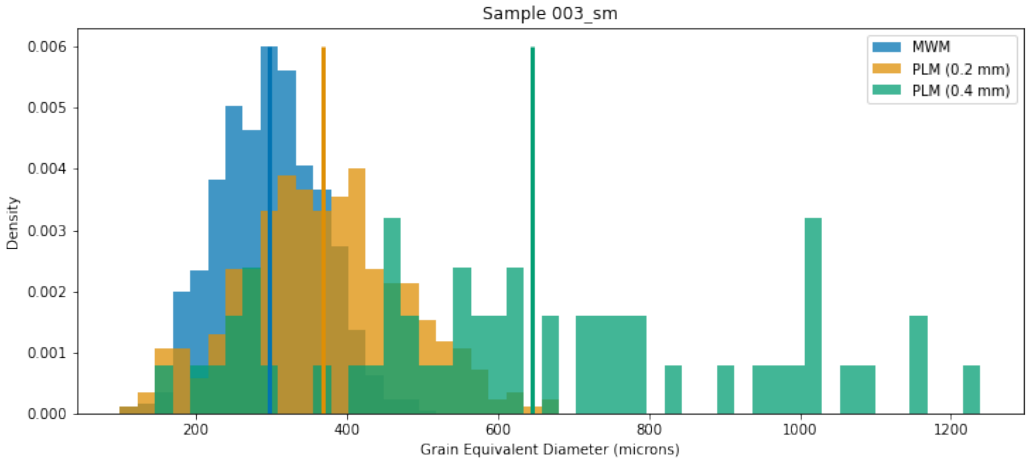

In addition to the comparison between the MWM and the PLM method, we compared laboratory-made snow samples with different grain sizes and sintering times. The MWM was applied to samples 003_sm and 003_md to see how the grain-size distributions changed (Figure 8). The mean segmented grain size for sample 003_md is roughly 0.40 mm larger than sample 003_sm, which shows the MWM can segment variable grain sizes.

Figure 8. Grain-size distributions produced by the MWM for two different-sized snow samples.

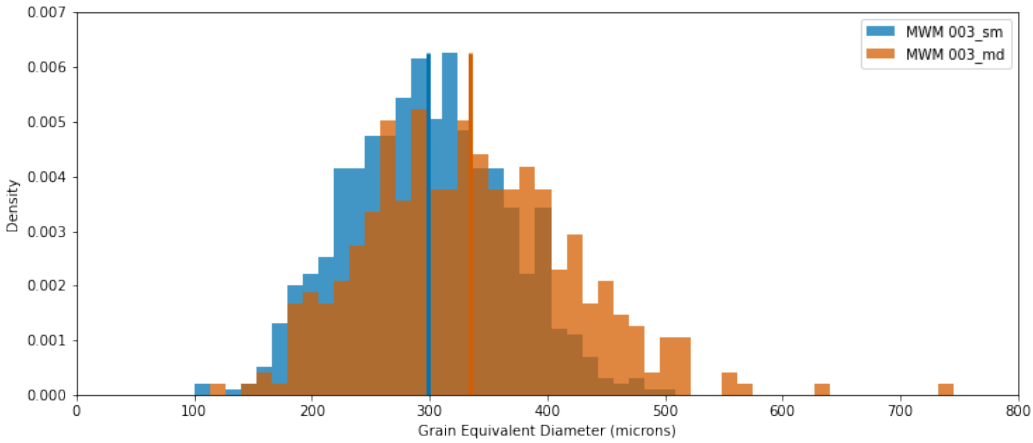

Figure 9 shows the distribution of bond radii derived from the segmented grains in Figure 7. These results also support the finding that the user-defined PLM approach can result in much different bond networks. Not only are there notably fewer bonds identified using the PLM function, but also the bonds are significantly larger because of the artificially large contact areas between the neighboring grains. Figure 10 shows the distribution of

bond radii between samples 003_sm and 133_sm. Sample 133_sm, which sintered for 130 days longer than 003_sm, had a mean bond radius that was roughly 0.20 mm larger than that of 003_sm. This demonstrates that with samples of similar grain size, the variable bond size can still be captured using the results of the MWM segmentation.

Figure 9. Distribution of bond radii identified within the segmented results using different segmentation methods. The MWM and the PLM (min distance 0.2 mm) produce similar distributions. However, the PLM (min distance 0.4 mm) produced many thick bonds.

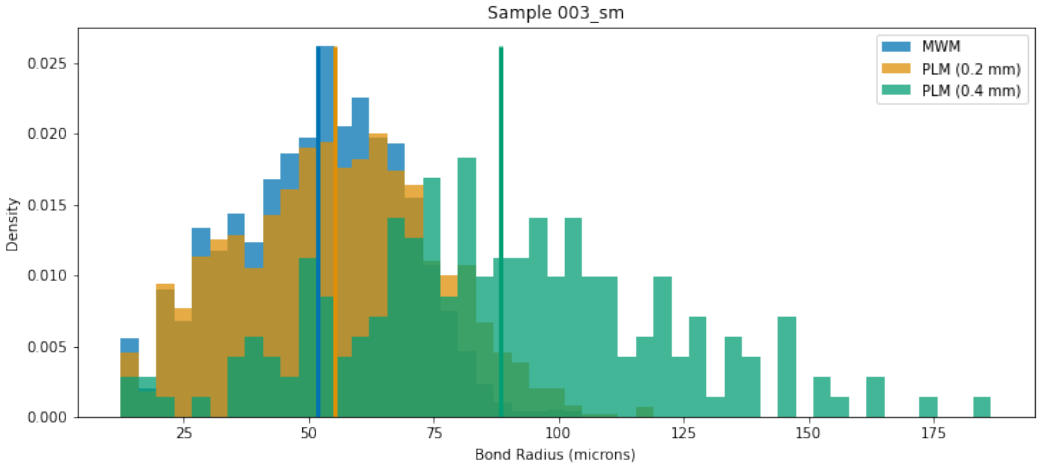

Figure 10. Distribution of bond radii for samples 003_sm and 133_sm identified using the MWM.

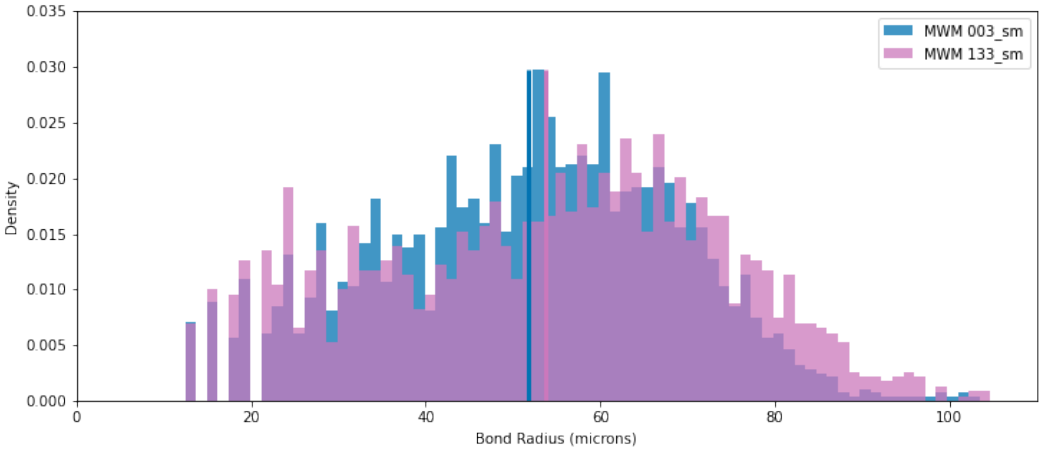

The final segmentation will also dictate how the sintered bonds are oriented. Bond orientation likely plays a role in the overall mechanical strength of snow; thus, it is important to see how the orientations vary based on the different segmentation results. Figure 11 shows the distribution of bond orientations produced with each segmentation method. The orientation is measured as the angle between the bond and the axis of

compression (*z*-direction). In this example, it is clear that the bond orientations generally do not change for each segmentation method, with most of the bonds oriented close to perpendicular to the axis of compression.

Figure 11. Distribution of bond orientations within the segmented results using different segmentation methods. The orientation is measured as the angle between the bond vector and a vector pointing in the *z*-direction (axis of compression). All three segmentation approaches produce very similar bond orientations.

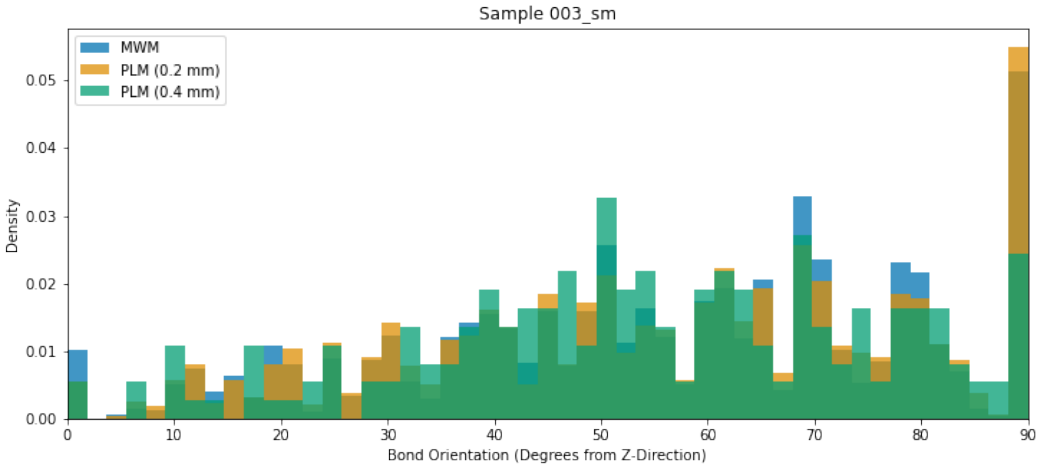

5 Conclusions

The goal of this study was to develop and test a methodology to extract sintered snow properties from microCT imagery, which can be used to initialize numerical models. More specifically, we developed the MWM to identify seed points for watershed segmentation. We then used the resultant watershed segmentation to identify and characterize individual snow grains and the sintered bonds between them. The MWM was tested against a common seed-point PLM to see which method produced more-realistic grain shapes and bond sizes. Qualitatively, the MWM produced segmented grains that aligned with visually distinguishable snow grains, whereas the PLM method produced primarily large-grain clusters that appeared to combine multiple individual snow grains. The grain-size distribution of the different methodologies shows this quantitatively—95% of the MWM grains were smaller than the sieve size used to make the sample, whereas both PLM grain sets had large numbers of grains that were larger than the sieve size. This result, as well as the comparison in Figure 6, illustrates how the PLM approach requires parameter tuning to generate realistic results, which can be time intensive and subjective.

We also tested the MWM and its ability to distinguish between samples made with different grain sizes. The grain-size distributions in Figure 8 show that the laboratory-made medium-grain-size sample (450–800 μm) had a segmented average grain size that was larger than the laboratory-made sample with the small grain size (<450 μm). The segmented grain-size distribution of the medium-sized sample did not fit the expected range as closely as the small sample. This will likely require some additional fine-tuning to produce results that more closely match the real sample. We also compared the bond-size distribution for each segmentation method. Because the bond sizes are directly correlated to the grain-size distributions and number of grains, the MWM produced bonds that were notably smaller and more abundant than either result derived from the PLM method. Regardless of the segmentation method, the bond orientation distributions all were fairly similar, with a large amount of the bonds oriented horizontally. In future work, we will test the sensitivity of the segmented results to the defined gradient threshold. The results of this analysis indicate that the MWM produces more-accurate grain sizes than the PLM method, and it is far less subjective as there is no a priori knowledge or assumptions required.

References

Attene, M. 2010. "A Lightweight Approach to Repairing Digitized Polygon Meshes." *The Visual Computer* 26:1393–1406. https://doi.org/10.1007/s00371-010-0416-3.

Baldwin, Christopher A., Andrew J. Sederman, Michael D. Mantle, Paul Alexander, and Lynn F. Gladden. 1996. "Determination and Characterization of the Structure of a Pore Space from 3D Volume Images." *Journal of Colloid and Interface Science* 181 (1): 79–92. https://doi.org/10.1006/jcis.1996.0358.

Bobillier, Grégoire, Bastian Bergfeld, Achille Capelli, Jürg Dual, Johan Gaume, Alec van Herwijnen, and Jürg Schweizer. 2020. "Micromechanical Modeling of Snow Failure." *The Cryosphere* 14 (1): 39–49. https://doi.org/10.5194/tc-14-39-2020.

Boykov, Yuri, Olga Veksler, and Ramin Zabih. 2001. "Fast Approximate Energy Minimization via Graph Cuts." *IEEE Transactions on Pattern Analysis and Machine Intelligence* 23 (11): 1222–1239. https://doi.org/10.1109/34.969114.

Brzoska, J. B., B. Lesaffre, C. Coléou, K. Xu, and R. A. Pieritz. 1999. "Computation of 3D Curvatures on a Wet Snow Sample." *The European Physical Journal Applied Physics* 7 (1): 45–57. https://doi.org/10.1051/epjap:1999198.

Chen, Si, and Ian Baker. 2010. "Evolution of Individual Snowflakes during Metamorphism." *Journal of Geophysical Research: Atmospheres* 115 (D21): D21114 . https://doi.org/10.1029/2010JD014132.

Coleou, Cecile, Bernard Lesaffre, Jean-Bruno Brzoska, Wolfgang Ludwig, and Elodie Boller. 2001. "Three-Dimensional Snow Images by X-Ray Microtomography." *Annals of Glaciology* 32: 75–81. https://doi.org/10.3189/172756401781819418.

Dey, Tamal K., Joachim Giesen, and Samrat Goswami. 2003. "Shape Segmentation and Matching with Flow Discretization." In *Algorithms and Data Structures*, edited by F. Dehne, J. R. Sack, and M. Smid. Lecture Notes in Computer Science, 2748: 25–36. Berlin: Springer. https://doi.org/10.1007/978-3-540-45078-8_3.

Edens, M. Q., and R. L. Brown. 1995. "Measurement of Microstructure of Snow from Surface Sections." *Defence Science Journal* 45 (2): 107–116. https://doi.org/10.14429/dsj.45.4109.

Flin, Frédéric, and Jean-Bruno Brzoska. 2008. "The Temperature-Gradient Metamorphism of Snow: Vapour Diffusion Model and Application to Tomographic Images." *Annals of Glaciology* 49: 17–21. https://doi.org/10.3189/172756408787814834.

Gaume, Johan, Alec van Herwijnen, Guillaume Chambon, Karl W. Birkeland, and Jürg Schweizer. 2015. "Modeling of Crack Propagation in Weak Snowpack Layers Using the Discrete Element Method." *The Cryosphere* 9 (5): 1915–1932. https://doi.org/10.5194/tc-9-1915-2015.

Hagenmuller, Pascal, Guillaume Chambon, and Mohamed Naaim. 2015. "Microstructure-Based Modeling of Snow Mechanics: A Discrete Element Approach." *The Cryosphere* 9 (5): 1969–1982. https://doi.org/10.5194/tc-9-1969-2015.

Hagenmuller, Pascal, Guillaume Chambon, Frédéric Flin, Samuel Morin, and Mohamed Naaim. 2014. "Snow as a Granular Material: Assessment of a New Grain Segmentation Algorithm." *Granular Matter* 16 (4): 421–432. https://doi.org/10.1007/s10035-014-0503-7.

Hagenmuller, Pascal, Margret Matzl, Guillaume Chambon, and Martin Schneebeli. 2016. "Sensitivity of Snow Density and Specific Surface Area Measured by Microtomography to Different Image Processing Algorithms." *The Cryosphere* 10 (3): 1039–1054. https://doi.org/10.5194/tc-10-1039-2016.

Johnson, Jerome B, and Mark A Hopkins. 2005. "Identifying Microstructural Deformation Mechanisms in Snow Using Discrete-Element Modeling." *Journal of Glaciology* 51 (174): 432–442. https://doi.org/10.3189/172756505781829188.

Kabore, B. Wendlassida, and Bernhard Peters. 2020a. "Micromechanical Model for Sintering and Damage in Viscoelastic Porous Ice and Snow. Part I: Model and Calibration." *International Journal of Solids and Structures* 185–186: 324–333. https://doi.org/10.1016/j.ijsolstr.2019.08.038.

Kabore, B. Wendlassida, and Bernhard Peters. 2020b. "Micromechanical Model for Sintering and Damage in Viscoelastic Porous Ice and Snow. Part II: Validation." *International Journal of Solids and Structures* 185–186:281–291. https://doi.org/10.1016/j.ijsolstr.2019.08.036.

Kabore, B. Wendlassida, Bernhard Peters, Mark Michael, and Francois Nicot. 2021. "A Discrete Element Framework for Modeling the Mechanical Behaviour of Snow—Part I: Mechanical Behaviour and Numerical Model." *Granular Matter* 23 (2): 42. https://doi.org/10.1007/s10035-020-01083-1.

Kaempfer, T. U., and M. Schneebeli. 2007. "Observation of Isothermal Metamorphism of New Snow and Interpretation as a Sintering Process." *Journal of Geophysical Research: Atmospheres* 112 (D24). https://doi.org/10.1029/2007JD009047.

Kaempfer, T. U., M. Schneebeli, and S. A. Sokratov. 2005. "A Microstructural Approach to Model Heat Transfer in Snow." *Geophysical Research Letters* 32 (21): L21503. https://doi.org/10.1029/2005GL023873.

Krol, Quirine, and Henning Löwe. 2016. "Relating Optical and Microwave Grain Metrics of Snow: The Relevance of Grain Shape." *The Cryosphere* 10 (6): 2847–2863. https://doi.org/10.5194/tc-10-2847-2016.

Langlois, A., B. Montpetit, A. Roy, and M. Durocher. 2020. "Presenting Snow Grain Size and Shape Distributions in Northern Canada Using A New Photographic Device Allowing 2D and 3D Representation of Snow Grains." *Frontiers in Earth Sciences* 7:347. https://doi.org/10.3389/feart.2019.00347.

Liang, Z., M. A. Ioannidis, and I. Chatzis. 2000. "Geometric and Topological Analysis of Three-Dimensional Porous Media: Pore Space Partitioning Based on Morphological Skeletonization." *Journal of Colloid and Interface Science* 221 (1): 13–24. https://doi.org/10.1006/jcis.1999.6559.

Lundy, Christopher, and Edward E. Adams. 1998. "Nondestructive collection of natural snow specimens for use with ct scan analysis." In *Proceedings of ISSW '98, International Snow Science Workshop*, 27 September–1 October 1998, Sunriver, Oregon, 208–213. https://arc.lib.montana.edu/snow-science/item/1491.

Mangan, Alan P., and Ross T. Whitaker. 1999. "Partitioning 3D Surface Meshes Using Watershed Segmentation." IEEE Transactions on Visualization and Computer Graphics 5 (4): 308–321. https://doi.org/10.1109/2945.817348.

Mulak, Dominika, and Johan Gaume. 2019. "Numerical Investigation of the Mixed-Mode Failure of Snow." Computational Particle Mechanics 6 (3): 439–447. https://doi.org/10.1007/s40571-019-00224-5.

Ogawa, Naohisa, Frederic Flin, and Jean Bruno Brzoska. 2006. "Representation of two Curvatures of Surface and Its Application to Snow Physics." *Memoirs of the Hokkaido Institute of Technology* 34:81–87.

Penrose, Mathew D. 2008. "Growth and Roughness of the Interface for Ballistic Deposition." *Journal of Statistical Physics* 131 (2): 247–268. https://doi.org/10.1007/s10955-008-9507-1.

Peters, Bernhard, B. Wendlassida Kabore, Mark Michael, and Francois Nicot. 2021. "A Discrete Element Framework for Modeling the Mechanical Behaviour of Snow Part II: Model Validation." *Granular Matter* 23 (2): 1–15. https://doi.org/10.1007/s10035-020-01084-0.

Schleef, Stefan, Henning Löwe, and Martin Schneebeli. 2014. "Hot-Pressure Sintering of Low-Density Snow Analyzed by X-Ray Microtomography and In Situ Microcompression." *Acta Materialia* 71:185–194. https://doi.org/10.1016/j.actamat.2014.03.004.

Serra, Jean Paul Frédéric. 1983. *Image Analysis and Mathematical Morphology*. New York: Academic Press.

Sullivan, C. Bane, and Alexander A. Kaszynski. 2019. "PyVista: 3D Plotting and Mesh Analysis through a Streamlined Interface for the Visualization Toolkin (VTK)." *Journal of Open Source Software* 4 (37): 1450. https://doi.org/10.21105/joss.01450.

Theile, T., and M. Schneebeli. 2011. "Algorithm to Decompose Three-Dimensional Complex Structures at the Necks: Tested on Snow Structures." *IET Image Processing* 5 (2): 132–140. https://doi.org/10.1049/iet-ipr.2009.0410.

van der Walt, Stéfan, Johannes L. Schönberger, Juan Nunez-Iglesias, François Boulogne, Joshua D. Warner, Neil Yager, Emmanuelle Gouillart, and Tony Yu. 2014. "scikit-image: Image Processing in Python." *PeerJ* 2:e453.

Wang, Xi, David Coeurjolly, and Frédéric Flin. 2014. "Digital Flow for Shape Decomposition: Application to 3-D Microtomographic Images of Snow." *Pattern Recognition Letters* 45: 181–188. https://doi.org/10.1016/j.patrec.2014.03.005.

Wang, Xi, Luc Gillibert, Frédéric Flin, and David Coeurjolly. 2012. "Curvature-Driven Volumetric Segmentation of Binary Shapes: An Application to Snow Microstructure Analysis." In *Proceedings of the 21st International Conference on Pattern Recognition (ICPR2012)*, 11–15 November, Tsukuba, Japan, 742–745. https://ieeexplore.ieee.org/document/6460241.

Willibald, Carolin. 2021. "Ice Spheres in Snow Mechanics: Microstructural Analyses, Experiments, and Simulations." PhD thesis, ETH Zurich. https://doi.org/10.3929/ethz-b-000472170.

Willibald, Carolin, Sophia Scheuber, Henning Löwe, Jürg Dual, and Martin Schneebeli. 2019. "Ice Spheres as Model Snow: Tumbling, Sintering, and Mechanical Tests." *Frontiers in Earth Science* 7:229. https://doi.org/10.3389/feart.2019.00229.

Zhang, Yan, J. Paik, Andreas Koschan, Mongi A. Abidi, and David Gorsich. 2002. "Simple and Efficient Algorithm for Part Decomposition of 3-D Triangulated Models Based on Curvature Analysis." In *Proceedings, International Conference on Image Processing*, 22–25 September, Rochester, NY, III-273–III-276. https://doi.org/10.1109/ICIP.2002.1038958.

REPORT DOCUMENTATION PAGE

Form Approved

OMB No. 0704-0188

1. REPORT DATE (DD-MM-YYYY)	2. REPORT TYPE	3. DATES COVERED (From - To)
September 2022	Final Technical Report (TR)	FY21–FY23

4. TITLE AND SUBTITLE

Extracting Sintered Snow Properties from MicroCT Imagery to Initialize a Discrete Element Method Model

5a. CONTRACT NUMBER

5b. GRANT NUMBER

5c. PROGRAM ELEMENT

0601102A

6. AUTHOR(S)

Taylor S. Hodgdon, Brendan A. West, Julie T. Parno, Theodore W. Letcher, Zoe R. Courville, and Lauren B. Farnsworth

5d. PROJECT NUMBER

AB2

5e. TASK NUMBER

SAB202

5f. WORK UNIT NUMBER

7. PERFORMING ORGANIZATION NAME(S) AND ADDRESS(ES)

US Army Engineer Research and Development Center (ERDC)
Cold Regions Research and Engineering Laboratory (CRREL)
72 Lyme Road
Hanover, NH 03755-1290

8. PERFORMING ORGANIZATION REPORT NUMBER

ERDC/CRREL TR-22-15

9. SPONSORING / MONITORING AGENCY NAME(S) AND ADDRESS(ES)

Headquarters, US Army Corps of Engineers
Washington, DC 20314-1000

10. SPONSOR/MONITOR'S ACRONYM(S)

USACE

11. SPONSOR/MONITOR'S REPORT NUMBER(S)

12. DISTRIBUTION / AVAILABILITY STATEMENT

Approved for public release; distribution is unlimited.

13. SUPPLEMENTARY NOTES

14. ABSTRACT

Modeling snow's mechanical behavior is important for many cold regions engineering problems. Because snow's microstructure plays a significant role in its mechanical response, it is imperative to initialize models with accurate bond characteristics and realistic snow-grain geometries to precisely capture the microstructure interactions.

Previous studies have processed microcomputed tomography scans of snow samples with a watershed method to extract grain geometries. This approach relies on identification of seed points to segment each grain. Our new methodology, called the "moving window method," does not require prior knowledge of the snow-grain-size distribution to identify seed points. We use the interconnectivity of the segmented grains to identify bond characteristics. We compare the resultant grain-size and bond-size distributions to the known grain sizes of the laboratory-made snow samples. The grain-size distributions from the moving window method closely match the known grain sizes, while both results from the traditional method produce grains that are too large. We propose that the bond network identified using the traditional method underestimates the number of bonds and overestimates bond radii. Our method allows us to segment realistic snow grains and their associated bonds, without prior knowledge of the samples, from which we can initialize numerical models of the snow.

15. SUBJECT TERMS

Discrete element method, Microcomputed tomography, Microstructure, Snow, Snow mechanics

16. SECURITY CLASSIFICATION OF:			17. LIMITATION OF ABSTRACT	18. NUMBER OF PAGES	19a. NAME OF RESPONSIBLE PERSON
a. REPORT	b. ABSTRACT	c. THIS PAGE			19b. TELEPHONE NUMBER (include area code)
Unclassified	Unclassified	Unclassified	SAR	32	